Applied Clay Science 75-76 (2013) 52–59

Contents lists available at SciVerse ScienceDirect

Applied Clay Science

journal homepage: www.elsevier.com/locate/clay

Research paper

Nanocomposites of halloysite and polylactide

Mingxian Liu, Yun Zhang, Changren Zhou *

Department of Materials Science and Engineering, Jinan University, Guangzhou 510632, China

ARTICLE INFO

Article history:
Received 20 March 2012
Received in revised form 19 February 2013
Accepted 24 February 2013
Available online xxxx

Keywords:
Halloysite
Polylactide
Nanocomposite
Mechanical property
Interaction
Crystallization

ABSTRACT

Naturally occurred halloysite (Hal) nanotubes compounded with polylactide (PLA) via melt mixing formed biodegradable and biocompatible clay polymer nanocomposites (CPN). The hydrogen bonding interactions between Hal and PLA were confirmed by Fourier transform infrared spectroscopy (FTIR). The modulus, strength and toughness of the Hal-PLA nanocomposites were substantially higher than those of neat PLA. Storage modulus and glass transition temperature of the Hal-PLA nanocomposites also increased with Hal loading as observed by dynamic mechanical analysis. The scanning electron microscopy (SEM) and transmission electron microscopy (TEM) results showed that Hal was uniformly dispersed and oriented in the CPN. X-ray diffraction (XRD) of the CPN showed the absence of Hal reflection at around 20°, indicating interactions of the PLA molecular chains in the interlayer space of Hal. Hal could nucleate PLA, leading to the decreased cold crystallization temperature and increased crystallinity. The vicat softening temperature and the degradation temperature of the CPN increased with Hal loading. Owing to the high performance and biocompatibility of the CPN, the prepared Hal-PLA nanocomposites had potential applications in biodegradable plastic and biomedical areas.

1. Introduction

Polylactic acid or polylactide (PLA) was a biodegradable, biocompatible, and thermoplastic aliphatic polyester derived from renewable resources, such as corn starch, tapioca products and sugarcanes. It was widely used in biomedical and degradable plastic areas (Rasal et al., 2010). For many applications of PLA, for example, as the bone internal fixation material, its mechanical performance should be improved in order to meet the requirement for strength and modulus (Shikinami and Okuno, 1999). Synthesis of PLA with high molecular mass was an effective way to achieve this aim (Purnama and Kim, 2009), but it was hard to control and the cost was extremely high. An alternative method was addition biocompatible particles or fibers as reinforcing materials when preparing PLA nanocomposites. Many types of nanoparticles, such as carbon nanotubes (CNT), hydroxyl-apatite (HA), nanoclay, silica, zinc oxide, and POSS, were incorporated into PLA to improve the physical and mechanical properties (Singh and Ray, 2007). For example, incorporation of HA into PLA increased the mechanical properties and bioactivities (Shikinami and Okuno, 1999; Verheyen et al., 1992). The flexural strength and flexural modulus of PLA nanocomposites with 40 m% HA reached 270 MPa and 9.1 GPa respectively, which were higher than those of the cortical bone (Shikinami and Okuno, 1999). Blending organo montmorillonite (OMt) with PLA could form exfoliated clay polymer nanocomposites (CPN) whose mechanical properties were substantially higher than those of neat PLA (Ray and Bousmina, 2005). CNT or graphene could also improve the mechanical and thermal properties of PLA (Barrau et al., 2011; Ramontja et al., 2009; Xu et al., 2010). For these nanoparticles-filled PLA systems, numerous modification methods were proposed to improve the interfacial bonding, but the procedures were neither easy to handle nor environmental-friendly. In addition, the availability and biocompatibility of the nanofillers were highlighted for biomedical applications of PLA nanocomposites. Since many nanoparticles were toxic (Nel et al., 2006), such as carbon fullerenes, CNT, and metal oxides nanoparticles, the prepared PLA nanocomposites could not be directly utilized in biomedical area. Therefore, exploring simple method of preparing PLA nanocomposite with available and biocompatible nanoparticle was generally needed for expanding PLA's applications.

Halloysite nanotube (Hal) was a natural aluminosilicate ($Al_2Si_2O_5(OH)_4 \cdot nH_2O$), which had predominantly hollow tubular structure in submicrometer range with high aspect ratio (Joussein et al., 2005). The length of the nanotubes was in the range of 0.2–1.5 μm, while the inner diameter and the outer diameter of tubes was 10–30 nm and 40–70 nm respectively. Hal was commonly used as bioreactor (Shchukin et al., 2005), time-release capsule (Lvov et al., 2008), catalysts of polymer degradation (Cho et al., 2006), template (Wang et al., 2008; Zhang and Liu, 2008), and high-tech ceramic applications (Sumi et al., 1998) etc. In recent years, Hal was evaluated as one-dimensional nanofillers for polymers (Du et al., 2010). Due to the excellent hydrophilicity and small dimension of Hal, it was readily dispersed in water. Thanks to this feature of Hal, water soluble polymer-Hal nanocomposites could be prepared by solution mixing (Liu et al., 2007a). Hal aggregates were also easily separated in polymer molten by shear, so many polymers were mixed with Hal via

* Corresponding author. Fax: +86 20 8522 3271.
E-mail address: tcrz9@jnu.edu.cn (C. Zhou).

0169-1317/$ – see front matter © 2013 Elsevier B.V. All rights reserved.
http://dx.doi.org/10.1016/j.clay.2013.02.019

melt blending. The Hal-polymer nanocomposites exhibited a significant increase in mechanical and thermal properties (Du et al., 2010). Recently, study on the biocompatiblity of Hal was conducted for exploring its applications in biomaterials (Hughes and King, 2010; Qi et al., 2010; Vergaro et al., 2010; Zhou et al., 2009). Vergaro et al.(2010) investigated Hal's toxicity to various cells and the uptake process by the cells. The result demonstrated that Hal was cytocompatible and could be potentially used as biomaterials. As an alternative one-dimensional nanoparticles for CNT, Hal was cheap, abundantly available, environmental-friendly, mechanically strong and biocompatible (Lvov et al., 2008; Qiao et al., 2012). Therefore, using Hal for preparing biocompatible and biodegradable CPN was significant both in theory and practice (Cavallaro et al., 2011a,b).

Beforetime, PLA was limited to biomedical applications due to its high production cost. An innovation on the production process of PLA by Natureworks LLC Company significantly lowered the production price. This required further studies on its properties and potential applications as bio-based and degradable plastic to replace the traditional oil-based non-degradable plastic (Madhavan Nampoothiri et al., 2010). The present work aimed to incorporate the natural Hal into PLA by melt mixing to form a bionanocomposite. The enhancements in mechanical and thermal properties of PLA were correlated to the good dispersion of Hal and interactions between PLA and Hal. Both PLA and Hal were derived from nature, so the prepared Hal-PLA nanocomposites were totally green materials. Apart from using as degradable plastic, the potential application of Hal-PLA nanocomposites also could be expanded to drug carrier, since Hal had unique lumen structures which endowed its high loading efficiency and controlled release ability for drugs.

2. Experimental

2.1. Materials

Polylactide (PLA), with trade name of Ingeo™ 3051D, was purchased from Natureworks. The melt index was 14 g/10 min according to the standard of ASTM D1238. The halloysite came from the deposit of Hunan province, China, and was used without purification. The raw Hal showed a layer spacing of 7.2 Å indicating its high hydration state. The elementary composition of Hal by X-ray fluorescence was as follows (m%): SiO_2, 58.91; Al_2O_3, 40.41; Fe_2O_3, 0.275; and TiO_2, 0.071. The Brunauer–Emmett–Teller (BET) specific surface area of Hal was approximately 50.4 m^2/g.

2.2. Sample preparation

An open two-roll mill with heating unit was used to compound PLA and Hal. The mixing temperature and time was 155 °C and 5 min respectively. Then the samples were broken to pieces for injection molding by a universal kibbler under room temperature. The samples were then dried for 4 h under 60 °C and injection-molded at the temperature of 165 °C. The digit in the code of PLA0, PLA5, PLA10, PLA20, PLA30, and PLA40 represented the Hal parts per hundred of polymer (phr). The neat PLA sample was transparent, while it became opaque after the incorporation of Hal.

2.3. Sample characterization

FTIR spectra were recorded on a Brucker Vector 33 spectrometer. Neat PLA and Hal-PLA nanocomposites were hot melted and then coated on KBr pellets. Hal powder was mixed and pelleted with KBr. Thirty-two consecutive scans from 4000 to 400 cm^{-1} were taken and their average was stored. The resolution of the wavenumber was 2 cm^{-1}. The fractured surfaces of neat PLA and the CPN were prepared by snapping in a liquid nitrogen environment. Then the surfaces were plated with a thin layer of gold before inspection under scanning electron microscopy (SEM). The SEM observations were conducted with LEO1530 VP SEM machine. Transmission electron microscopy (TEM) analysis of Hal and the CPN was carried out with Philips Tecnai 10 TEM. Thin sections of the samples were cut using Leica EM UC6 ultramicrotome and the sections were supported by carbon-coated copper grid. Hal sample was ultrasonically dispersed in ethanol, and then a drop of sample dispersion was dropped onto a carbon-coated copper grid, which was then left to stand for 10 min before transferring it into the microscope. The accelerating voltage for TEM observation was 100 kV. Differential scanning calorimetry (DSC) was measured by NETZSCH DSC204 F1 using nitrogen as purging gas. For DSC measurement, the samples were heated to 200 °C at ramping rate of 10 °C/min. The samples were kept at 200 °C for 3 min to eliminate the thermal history before they were cooled down to 30 °C at ramping rate of 10 °C/min. Then the samples were again heated to 200 °C at ramping rate of 10 °C/min. The endothermic and exothermic flows were recorded as a function of temperature. The crystallinity of the PLA in the CPN was calculated according to the below equation.

$$Crystallinity(\%) = \frac{\Delta H_m - \Delta Hcc}{\Delta H_m^0 \times C} \quad (1)$$

where ΔH_m and ΔH_m^0 were the endothermic enthalpy of the samples and that of the 100% crystallized PLA (93 J/g (Fischer et al., 1973)) respectively. ΔH_{cc} was the enthalpies of cold crystallization. C was the PLA mass percentage (m%) in the Hal-PLA nanocomposites.

Specimens for the tensile, flexural, and impact testing were measured according to ISO 527: 1993, ISO 178: 1993 and ISO 180: 1993 respectively in Zwick/Roell Z005 Testing Machine and MTS ZBC50 tester (Shenzhen, China). The tensile and flexural tests were performed under a crosshead speed of 50 mm/min and 2 mm/min respectively, and the measured temperature was around 25 °C. At least five samples were measured and the average values and the standard deviation were reported. Dynamic mechanical analysis was conducted with a NETZSCH Instruments DMA 242 at an oscillation frequency and heating rate of 1.0 Hz and 5 °C/min respectively. The 3-point bending mode was selected and the experiments were conducted under air atmosphere. XRD profiles for samples were obtained using X-ray diffractometer (D8, Bruker Corporation) at room temperature. The CuKa radiation source was operated at 40 kV power and 40 mA current. The wavelength of the X-ray beam was 0.15418 nm, and the layer spacing of the samples were calculated according to the Bragg's equation. The scanning angle ranged from 2° to 50°. Thermogravimetric analysis (TGA) was carried out under N_2 atmosphere with TA Q5000 at the heating rate of 10 °C/min from room temperature to 600 °C. The vicat softening temperatures of the samples were determined using GOTECH HV-2000A Computer HDT/VICAT Tester. The heating rate was 1 °C/min. All the tests were repeated at least three times for reliable data.

3. Results and discussion

Hal was natural 1D nanomaterial that could be used as nanofiller for polymers. The as-used Hal particles had a cylindrical shape with hollow and open-ended tubular morphology (Fig. 1). The morphology was relatively uniform and the tubular quality was good. The inner and outer diameters of the Hal were in the range of 10–30 nm and 40–70 nm respectively, while the length of the tubes was in the range of 200 nm–1.5 μm. The calculated aspect ratio of Hal was ca. 20. The BET specific surface area of Hal was 50.4 m^2/g. The mean particle size of Hal in a 5 m% aqueous solution was 143 nm and its size ranged from 50 to 400 nm (Liu et al., 2007b). The raw Hal had uniform tubular morphology, high aspect ratio, high specific surface area and good dispersion ability in polymers. These features make Hal ideal as nanofillers for polymers (Du et al., 2010). In the following part, the interactions between Hal and PLA were investigated by FTIR and after

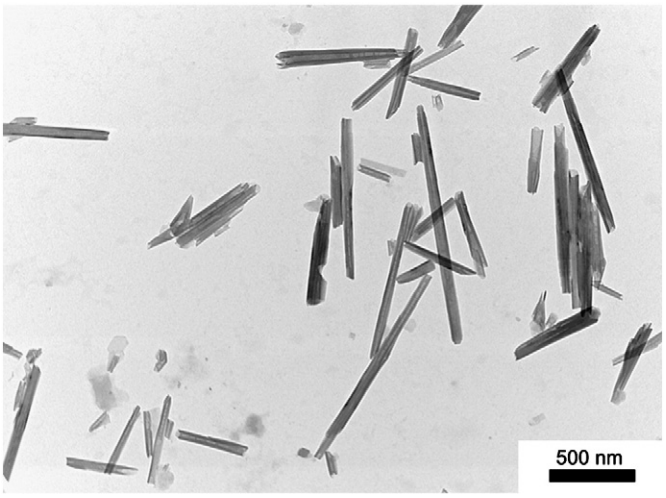

Fig. 1. TEM photos of the as-used Hal.

that the influence of Hal on the mechanical, morphological and thermal properties of Hal-PLA nanocomposites were examined in details.

The FTIR spectra were collected to examine the molecular interactions between PLA and Hal (Fig. 2). FTIR spectra of Hal exhibited two characteristic bands at around 3621 cm^{-1} and 3695 cm^{-1} which were assigned to the vibration of inner hydroxyl groups and the hydroxyl groups located at the octahedral surface of the nanotubes respectively (Yuan et al., 2008). There were two bands at 3501 cm^{-1} and 3665 cm^{-1} in the spectra of PLA, which could be attributed to the two terminal hydroxyl groups (–OH) of PLA (Matusik et al., 2011; Zhou et al., 2007). As expected, there were characteristic absorption bands of both Hal and PLA in the case of the Hal-PLA nanocomposites. The intensity of the bands at 3621 cm^{-1} and 3695 cm^{-1} increased proportionally to the amount of introduced Hal, which confirmed the presence of the nanotubes in the polymer matrix. However, these bands shifted to higher frequencies in the spectra of the Hal-PLA nanocomposites. For example, they appeared at around 3625 cm^{-1} and 3698 cm^{-1} in PLA40. The shift might be caused by hydrogen-bonding interactions between the carbonyl groups (C═O) of PLA and the hydroxyl groups of Hal. On the other hand, the hydroxyl groups of PLA could also interact with the Si–O–Si groups of Hal via hydrogen bonding interactions. This was confirmed by the blue-shift of the band at 3501 cm^{-1} assigned to hydroxyl groups of PLA in spectra of the Hal-PLA nanocomposites. In the region of 3000–1300 cm^{-1}, there were no absorption bands for Hal. The PLA spectrum in the region of 3000–1300 cm^{-1} could be characterized by

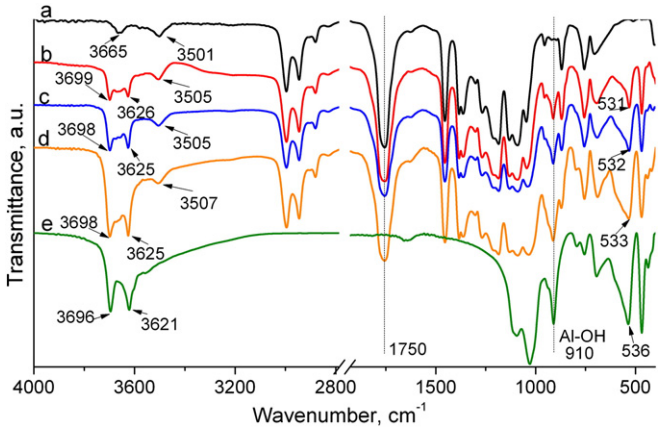

Fig. 2. FTIR spectra of PLA, Hal and Hal-PLA nanocompoites: (a) PLA, (b) PLA5, (c) PLA20, (d) PLA40 and (e) Hal.

absorption bands at 2996, 2946 and 2881 cm^{-1} arising from the C–H stretching vibrations of CH_3 and CH groups as well as a band ascribed to the stretching vibration of C═O groups at 1756 cm^{-1}, bending vibration of CH_3 groups at 1454 cm^{-1}, and absorption bands at 1384 and 1364 cm^{-1} arising from the C–H deformation and asymmetric/symmetric bending, respectively (Bocchini et al., 2010). In this region, the intensities and the position of the PLA characteristic peaks nearly did not change with the addition of Hal. In the region of 1300–500 cm^{-1}, the characteristics absorption bands of Hal and PLA were overlapped. For example, the main absorbance bands at 1094 and 1029 cm^{-1} associated with the stretching of Si–O–Si of Hal were overlapped by the bands at 1091 cm^{-1} and 1042 cm^{-1} of C–O–C and C–CH_3 of PLA. Therefore, it was hard to discriminate the changes of the bands for these samples in this region. In the spectra of the Hal-PLA nanocomposites, a shift was observed only for the absorption band at 536 cm^{-1} associated with the deformation of Al–O–Si groups of Hal. This shift to lower wavenumber could be attributed to the hydrogen bonding interactions between Hal and PLA. The hydrogen bonding interactions between PLA and other nanoparticles were also confirmed by FTIR in other systems (Matusik et al., 2011; Zhou et al., 2007). The interactions between Hal and PLA probably contributed to the enhanced mechanical and thermal properties of CPN compared to the neat PLA.

The influence of Hal on the mechanical properties of PLA was firstly investigated. Hal significantly improved both tensile and flexural properties of PLA, and the increase was proportional with the loading of Hal (Fig. 3 and Table 1). For example, the tensile strength, flexural strength and flexural modulus of Hal-PLA nanocomposites with 30 phr Hal were 74.1 MPa, 108.3 MPa and 6.56 GPa, which were 34%, 25%, and 116% higher than those of the neat PLA respectively. Three types of reinforcing effect by nanoparticles for PLA were reported in the references. (1) Decreased strength with the addition of nanoparticles; for example, incorporation of POSS to PLA resulted in decreased tensile strength (Turan et al., 2011). About 50% decrease in tensile strength was also observed in the case of ZnO-PLA nanocomposites with of 2–3 m% untreated nanoscale ZnO (Murariu et al., 2011). (2) Strength nearly were not changed by nanoparticles; For example, incorporation of multi-walled carbon nanotubes (MWCNT) into PLA led to slightly change in tensile strength (Ramontja et al., 2009). (3) Increased strength and modulus by nanoparticles; For example, the maximum tensile strength and Young's modulus of PLA with nanosilica were obtained at a silica content of 2 m%, which were 15% and 37.4% increment compared with neat PLA respectively (Kontou et al., 2011). There were 56% and 15% increase in the flexural strength and flexural modulus respectively for the Mt-PLA nanocomposites compared with neat PLA (Ray and Okamoto, 2003). The differences of reinforcing effect for PLA arose from the structural characteristics of nanoparticles, dispersion state, and interfacial interactions in these systems. Comparing with other nanoparticles, Hal exhibited better reinforcing ability for PLA in term of the mechanical properties. The excellent reinforcing effect of Hal on PLA could be attributed to (i) the uniformly distributed rigid nanotubes in PLA matrix (SEM and TEM result below) and (ii) the hydrogen bonding interactions between Hal and PLA. But in the case of Hal-PLA nanocomposites with relatively high Hal loading (PLA40), the tensile and flexural properties started to decrease. This could be attributed to the presence of the aggregated Hal in the polymer matrix as shown in morphology results below. The aggregated Hal could act as the stress-centralized points, leading to the deteriorated properties.

In addition, the toughness of PLA was improved by Hal. The impact strength for all the Hal-PLA nanocomposites was higher than that of neat PLA, especially when the loading of Hal less than 20 phr. Small quantity of Hal could improve the toughness of PLA significantly. For instance, the impact strength of the Hal-PLA nanocomposites with 10 phr Hal was 32.3 J/m, which was 70% higher than that of neat PLA. Another indicator of toughness was the elongation at break for the tensile testing. The elongation at break of the Hal-PLA nanocomposites with Hal less than 20 phr was higher than that of

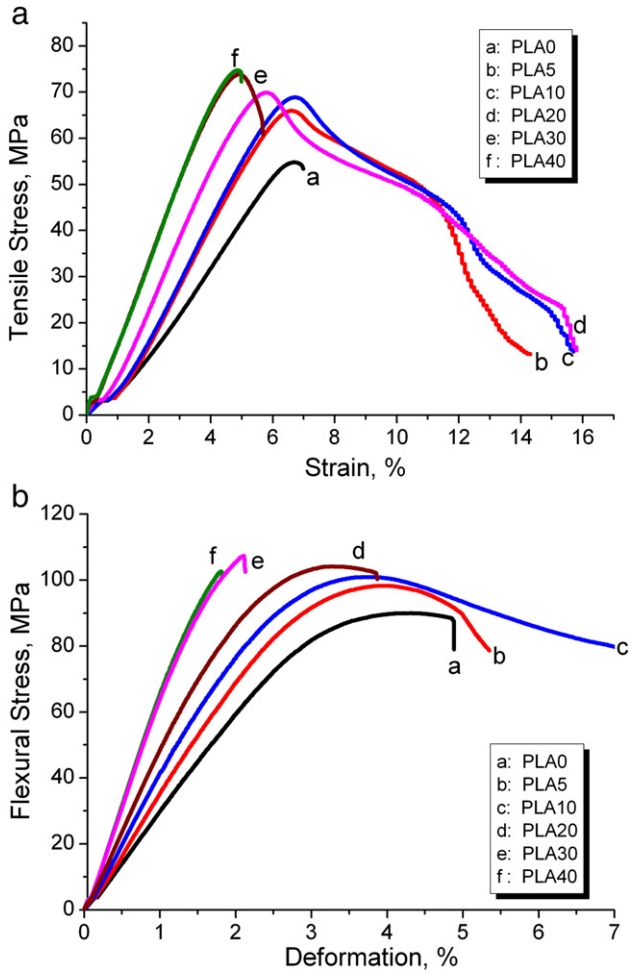

Fig. 3. Tensile (a) and flexural (b) strain–stress curves of PLA and Hal-PLA nanocomposites.

neat PLA (Fig. 3a), which was consistent with the impact test results. Small quantity of Hal could act as plasticizer of PLA, which distributed the impact energy during the fracture. The decreased toughness of the Hal-PLA nanocomposites with relatively high Hal loading should be attributed to the weakened interfacial interactions at high loadings of nanoparticles. This result was in agreement with the previous result of Mt-PLA nanocomposites, in which the brittle–toughness transition point appeared at 2.5 m% of the filler content (Jiang et al., 2007). Addition of nanoparticles to PLA for improving the toughness was widely reported (Anderson et al., 2008). The mechanical performance of Hal-PLA nanocomposites could be further improved via surface modification of Hal, for example, grafting PLA chains on the surface of Hal, which could increase the interfacial bonding.

Dynamic mechanical analysis (DMA) was used to evaluate the viscoelastic properties of Hal-PLA nanocomposites below and around the glass transition. The storage modulus significantly increased with the loading of Hal especially before the glass transition (Fig. 4a). For example, the storage modulus of PLA40 at 37 °C was 9.12 GPa, which was 143% higher than that of neat PLA. The reasons of the increase of storage modulus by Hal could be attributed to the following facts. Firstly, the interactions between polymer matrix and nanofillers could restrict the mobility of polymer chains adsorbed on the surface of Hal, leading to the formation of a stiffened interphase. Secondly, owing to the formation of Hal networks within the PLA matrix at high loading, the high modulus of Hal was also involved in the increased storage modulus of Hal-PLA nanocomposites. These two aspects were affected by dispersion, concentration, and degree of exfoliation of Hal. The well dispersion of Hal and the formation of Hal networks at high Hal loadings, shown in the morphology results below, contributed to the increased storage modulus. The temperature at the peak of tan δ curve was considered as the glass transition temperature (T_g) of the material. T_g of the Hal-PLA nanocomposites increased consistently with the loading of Hal (Fig. 4b). The maximum T_g was 82.5 °C (PLA40), which was 15.6 °C higher than that of neat PLA. This phenomenon suggested the presence of the interactions between Hal with the PLA chains, and the interactions restricted the mobility of the polymer chains during the glass transition. The low heat distortion temperature of PLA was a disadvantage compared with the polyolefines. The increased T_g suggested that the Hal-PLA nanocomposites could tolerate higher temperature than the neat PLA could.

Table 1
Mechanical properties of Hal-PLA nanocomposites (data in the parentheses indicates the standard deviations).

Samples	Tensile strength MPa	Elongation at break %	Flexural strength MPa	Flexural modulus GPa	Impact strength J/m
Neat PLA	55.2 (1.2)	7.0 (0.3)	86.7 (1.2)	3.04 (0.13)	19.0 (0.6)
PLA5	66.7 (1.4)	14.3 (0.5)	95.8 (3.4)	3.61 (0.02)	31.4 (0.5)
PLA10	68.6 (0.5)	15.7 (0.8)	99.9 (1.1)	4.25 (0.07)	32.3 (1.3)
PLA20	69.5 (0.8)	15.8 (0.8)	104.0 (0.3)	4.96 (0.07)	26.2 (2.4)
PLA30	74.1 (0.9)	5.7 (0.4)	108.2 (3.2)	6.56 (0.06)	24.9 (2.2)
PLA40	75.1 (0.7)	5.0 (0.2)	102.7 (2.5)	6.78 (0.20)	22.9 (1.6)

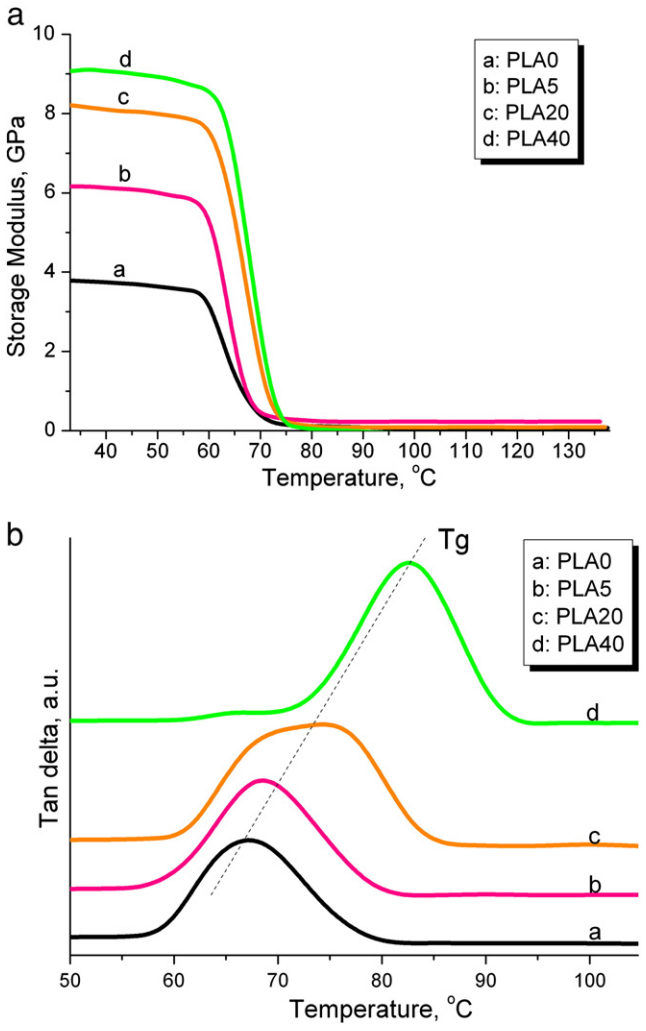

Fig. 4. Storage modulus (a) and tan δ (b) curves for PLA and Hal-PLA nanocomposites by dynamic mechanical analysis.

To understand the changes bring to PLA in mechanical performance by the addition of Hal, the microstructures of the Hal-PLA nanocomposites were observed by SEM and TEM. The neat PLA showed a glossy and ordered morphology of its fracture surface, indicating the typical brittle fracture during the cryofracturing process (Fig. 5). Hal was dispersed in the PLA matrix uniformly and the dispersion was nearly independent of the loading of Hal. The well dispersion of Hal in PLA could be attributed to two reasons. Firstly, the tubular morphological character of Hal and the relatively weak tube-tube interactions made them easy to be dispersed in polymers by shear forces. Secondly, Hal could interact with PLA via hydrogen bonding interactions as illustrated previously, which also facilitated its dispersion. Another interesting phenomenon was that only the end faces of the nanotubes could be found in the fracture surface of the Hal-PLA nanocomposites. This could be explained by the orientation of Hal in the matrix under shear forces during processing. The individually separated and oriented Hal could bear the load via the interfaces during the mechanical fracture. As a result, the Hal-PLA nanocomposites exhibited much higher strength and modulus. The good dispersion of raw Hal in other polymer matrix was also found (Du et al., 2010). Cracks were found in the matrix (Fig. 5b), which was probably attributed to the decomposition of PLA under the accelerating voltages during the SEM observation.

TEM photos also confirmed the good dispersion and orientation of Hal in PLA (Fig. 6). Hal was oriented by the shear force during processing in PLA matrix. This was consistent with SEM results above and XRD results below. Since Hal belonged to natural clay mineral and was used without grading, the nanotubes in the PLA matrix were different in length and diameter. The length of the nanotubes in the Hal-PLA nanocomposites was in the range of 200 nm–1 μm, while the diameter was in 40–100 nm. However, all the tubes were uniformly dispersed in the PLA matrix especially for the samples with low Hal content. When increasing the loading of Hal, the individually separated Hal and aggregated Hal coexisted in the samples. The aggregation of Hal should be the origin for the decreased mechanical properties of the Hal-PLA nanocomposites with relatively high Hal loading (40 phr). In spite of

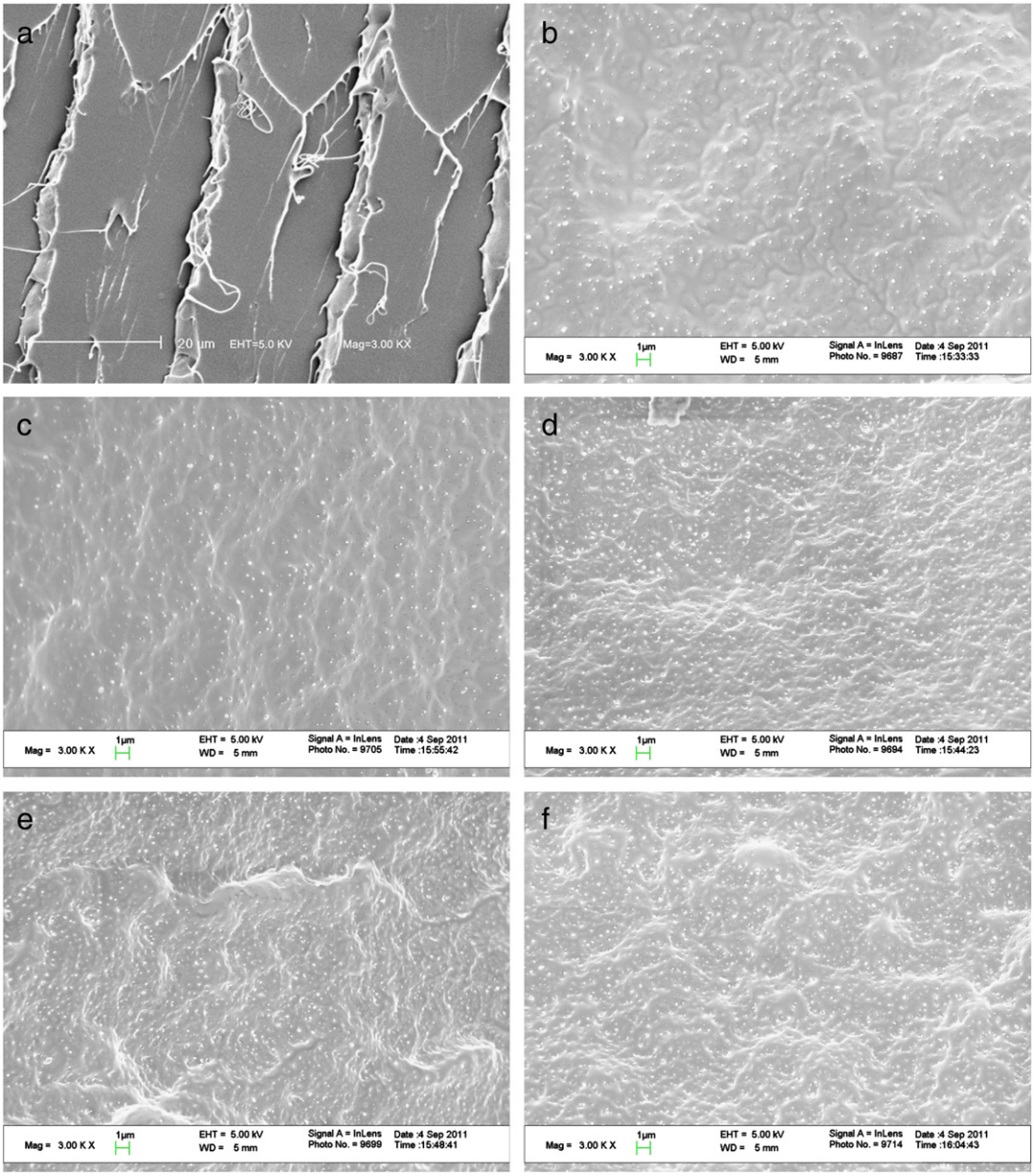

Fig. 5. SEM photos for fracture surface of Hal-PLA nanocomposites: (a) PLA0; (b) PLA5; (c) PLA10; (d) PLA20; (e) PLA30; and (f) PLA40. (The small white points in the photos were the individually dispersed nanotubes.).

this, Hal was superior to other nanoparticles for modification of PLA, as its could be used directly without complicated surface-treatment procedure. In contrast, a low degree of dispersion of raw Mt were found in the Mt-PLA nanocomposites (Bocchini et al., 2010).

To further illustrate the dispersion state of Hal and its interactions with PLA, XRD experiment was conducted. For neat PLA, only a broad scattering reflection, locating at around $2\theta = 16°$, was found in the XRD spectrum, indicating that it did not crystallize during the cooling step in the sample preparation process (Fig. 7) (Lim et al., 2008). The raw Hal showed a diffraction reflection at $2\theta = 12.26°$, corresponding to a basal spacing of 7.25 Å according to the Bragg equation. This basal reflection of 7.25 Å indicated that the used Hal was dehydrated. The intercalation of PLA into the interlayer of Hal did not occur, as the interlayer distances of Hal in all the samples remained unchanged. Therefore, PLA chains could not enter the interlayer of Hal during the processing. The polymer chains might be blocked by the strong hydrogen bonds between sheets of the nanotubes. Pretreatment of Hal by small molecules, such as dimethylsulfoxide (DMSO) or N-methylformamide, could lead to the intercalation of Hal by various guests (Joussein et al., 2005). Interestingly, the reflection of Hal at around 20° disappeared in all the Hal-PLA nanocomposites even with 5 phr Hal. This result suggested the presence of the interactions of polymer chains with the Hal. An explanation might be realized by attributing this to a preferential orientation of the nanotubes in the Hal-PLA nanocomposites like oriented tiles patterns which was induced by the shear force during processing. The orientation of the nanotubes was beneficial for the improvement of the mechanical and thermal properties of the Hal-PLA nanocomposites, since it led to 2D homogenization of the nanofillers in polymer matrix. Actually, the orientation of Hal was confirmed by the SEM and TEM results above. The change of the XRD pattern of Hal was in accordance with the results by the work of Rooj et al. (2010).

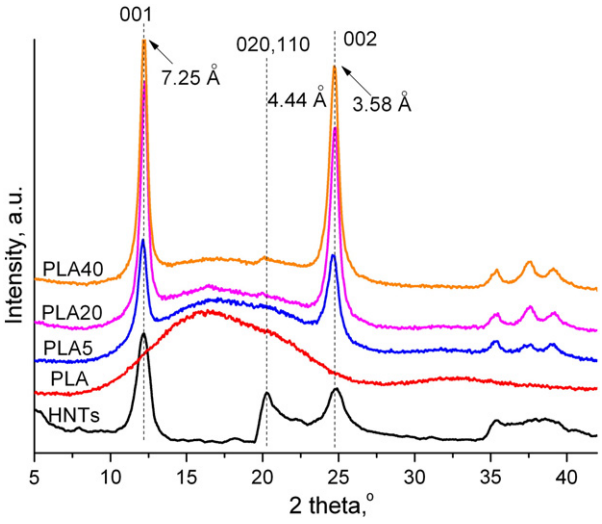

Fig. 7. XRD pattern of Hal, PLA, and Hal-PLA nanocomposites.

PLA was semicrystalline polymer and its mechanical and physical properties were governed by the crystal microstructure. The introduction of nanosized Hal affected the interactions among the PLA chains. The changed interfacial interactions in the CPN further affected the crystallization behavior and the physical structure of PLA. The cold crystallization peak of PLA (T_{cc}) shifted to lower temperature with Hal (Fig. 8 and Table 2). For example, the T_{cc} of PLA10 was 102.1 °C, which was 5.6 °C lower than that of neat PLA. This could be attributed to the nucleating effect of Hal in PLA cooling crystallization process. T_{cc}

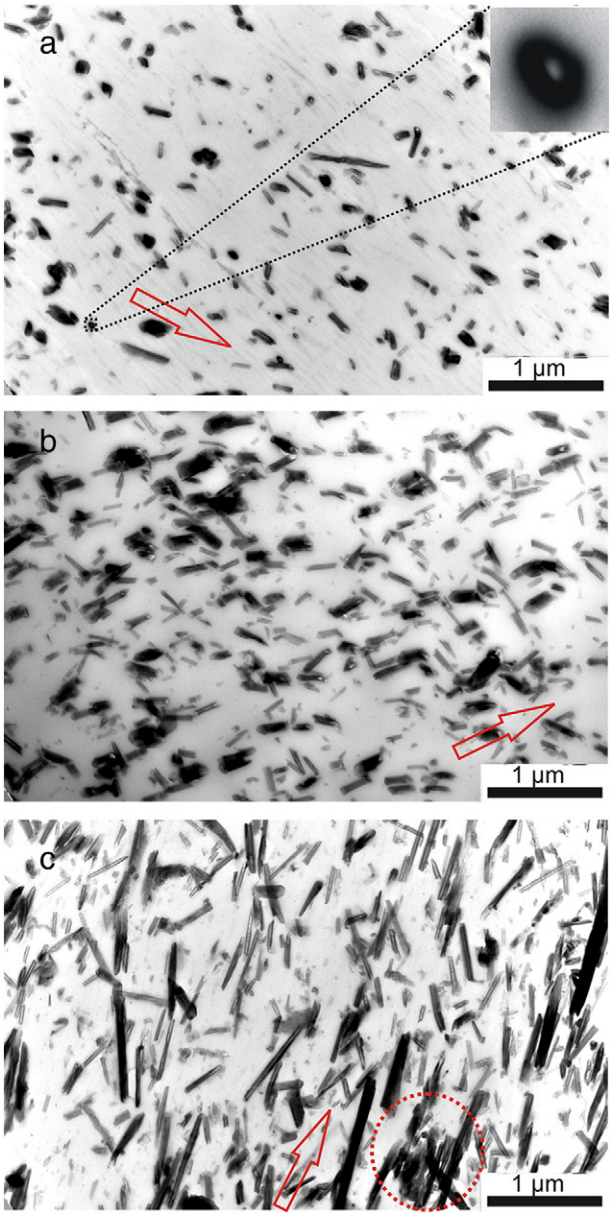

Fig. 6. TEM photos of Hal-PLA nanocomposites: (a) PLA5; (b) PLA20 and (c) PLA40. The arrows represent the orientation of the tubes. The circle in (c) represents the Hal aggregates. The inset in (a) represents the end faces of a tube in the PLA matrix.

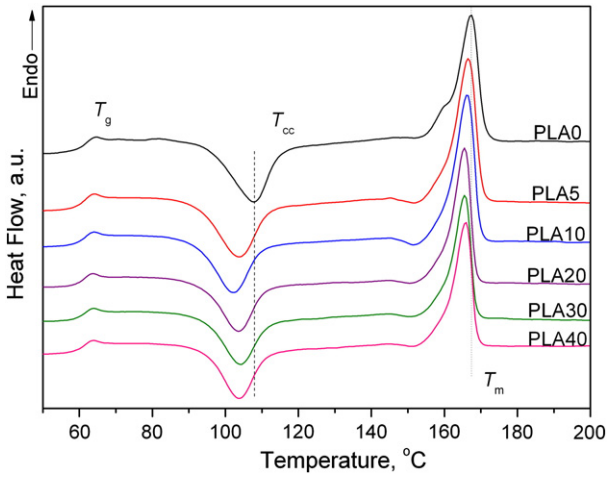

Fig. 8. DSC secondary heating curves of PLA and Hal-PLA nanocomposites with a heating rate of 10 °C/min.

Table 2
DSC and TGA data of the Hal-PLA composites with variable Hal content.

HNT content (phr)	T_g (°C)	T_{cc} (°C)	T_m (°C)	ΔH_m (J/g)	X_c[a] (%)	$T_{10\ wt.\%}$ (°C)	$T_{50\ wt.\%}$ (°C)
0	55.2	107.7	167.3	32.5	34.9	330.9	354.9
5	56.2	103.5	166.6	36.5	41.3	335.3	356.0
10	56.7	102.1	166.2	36.3	42.9	N/A	N/A
20	58.0	103.5	165.5	30.0	38.6	335.3	357.6
30	56.0	104.1	165.5	27.2	38.0	N/A	N/A
40	56.5	103.8	165.8	28.5	42.9	335.2	359.4

[a] The crystallinity of the samples was calculated by comparing the calibrated specific fusion heat with the standard fusion heat of PLA (93 J/g).

nearly did not depend upon the Hal content, which suggested that small amount of Hal could serve as an effective nucleating agent for PLA. On the other hand, the melting temperatures of the Hal-PLA nanocomposites were also lower than that for neat PLA. As Hal in the nanocomposites worked as a nucleating agent of PLA, the Hal-PLA nanocomposites could crystallize more quickly than neat PLA. However, the formed crystalline structure by the heterogeneous nucleation was less complete than that of PLA, for example, with thinner and/or less perfect crystalline lamella. As a consequence, the melting point of Hal-PLA nanocomposite was lower than that of PLA. A similar phenomenon was also found in CNT-PLA nanocomposites (Wu and Liao, 2007). The heterogeneous nucleation could lead to the increase of crystallinity of PLA. The crystallinities of the Hal-PLA nanocomposites were substantially higher than that of neat PLA (Table 2), although the increasing trend was not consistent. Similar results of the heterogeneous nucleation of nanosized particles for PLA were also found (Krikorian and Pochan, 2005; Xu et al., 2010). For instance, both CNT and graphene could serve as heterogeneous nucleation agents for PLA via the noncovalent interactions between the nanoparticles and polymer chains (Xu et al., 2010). A steplike change for all samples in the temperature range of 60–70 °C was assigned to the glass transition region of PLA (Fig. 8). The T_g of the Hal-PLA nanocomposite increased slightly with Hal content. The T_g determined by DSC was largely different from that determined by DMA. This difference should come from the different principles for determining T_g. For DMA method, the instrument measured the hysteresis between the applied force and the response of the macromolecular chains under repeated small-amplitude strains in a cyclic manner. But for DSC method, it measured the enthalpy change in heating or cooling process. Generally, it was considered that T_g determined by DMA was much more accurate than that obtained by DSC method (Sperling, 2006). The increased T_g was also attributed to the hydrogen bonding interactions between Hal and PLA.

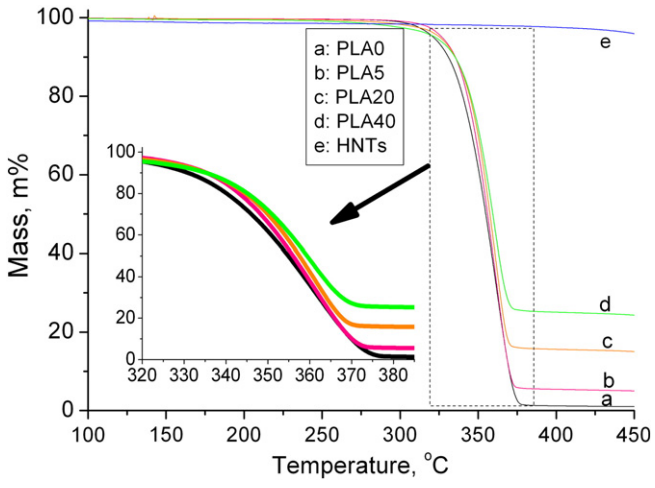

Fig. 9. TGA curves of PLA and Hal-PLA nanocomposites.

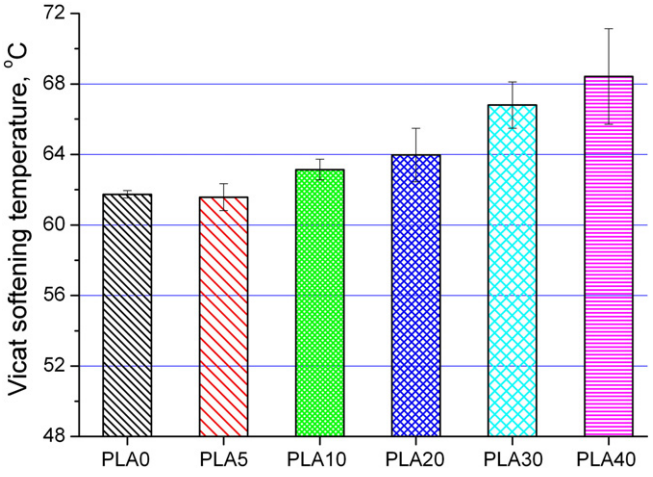

Fig. 10. Vicat softening temperature of PLA and Hal-PLA nanocomposites.

The thermal stability of PLA and Hal-PLA nanocomposites were compared by TGA method (Fig. 9 and Table 2). The neat PLA degraded without forming any residue, while the Hal-PLA nanocomposites left some residue related to the Hal. The thermal stability of the Hal-PLA nanocomposites increased comparing with that of neat PLA. The 10 m% and 50 m% mass loss temperatures of the Hal-PLA nanocomposites were higher than those of neat PLA. Since the degradation of Hal in the temperature region of 30–375 °C was negligible (2.1%), the mass loss of the Hal-PLA nancomposites in this temperature region was related to PLA. The increased thermal stability of the CPN could be attributed to the fact that the uniformly dispersed Hal in the matrix had a barrier effect against the volatile pyrolized products of PLA, eventually retarding thermal degradation of the CPN. However, the increase for thermal stability of PLA by Hal was very limited. The present TGA result was consistent with the previous reported thermal stability results of PLA/silica, PLA/Mt, and PLA/exfoliated graphite nanocomposites (Kim and Jeong, 2010; Kontou et al., 2011).

The vicat softening temperature of polymer-based nanocomposites was critical, as it represented the upper stability limit of the material without significant physical deformation under load and thermal effect. The influence of Hal on the vicat softening temperature of PLA was examined (Fig. 10). The vicat softening temperatures of PLA increased with the loading of Hal. For neat PLA, the softening temperature was 61.7 °C. The temperature increased to 68.4 °C for the Hal-PLA nanocomposite with 40 phr Hal. This result suggested that Hal could enhance the heat resistance of PLA. This could be explained by the facts that (i) the mechanical and heat energy could transfer from the PLA to the inorganic nanotubes and that (ii) the increased crystallinity of the PLA matrix by Hal increased the tolerance of heat. Other particles or fibers could also improve the thermal distortion temperature of PLA (Ray and Okamoto, 2003; Teng et al., 2011). The increased heat-resistant property of PLA was beneficial to its application in thermostable product.

4. Conclusions

Hal-PLA nanocomposites were prepared by melt compounding. The hydrogen bonding interactions between Hal and PLA were confirmed. Hal significantly increased the tensile, flexural, and impact properties of PLA. The storage modulus and glass transition temperature of PLA were also enhanced by Hal. Hal was uniformly dispersed and oriented in the PLA matrix. No intercalations of Hal by the PLA matrix were found, but Hal had preferential orientation in the Hal-PLA nanocomposites. Hal could act as nucleating agent for PLA, which led to decreased cold crystallization temperature and increased crystallinity. The vicat softening

temperature and thermal degradation temperature of PLA also increased by the addition of Hal. The prepared Hal-PLA nanocomposites were 100% nature-based materials, which could be potentially used as degradable plastic.

Acknowledgments

This work was financially supported by the Research Fund for the Doctoral Program of Higher Education of China (grant No. 20114401120003), the Key Laboratory of Rubber-plastics (Qingdao University of Science and Technology), Ministry of Education and the Key Laboratory of High Performance and Functional Polymeric Materials (South China University of Technology), Guangdong province, PR of China. The authors also thank Dr. Hau-To Wong for proof reading the manuscript.

References

Anderson, K.S., Schreck, K.M., Hillmyer, M.A., 2008. Toughening polylactide. Polymer Reviews 48, 85–108.
Barrau, S., Vanmansart, C., Moreau, M., Addad, A., Stoclet, G., Lefebvre, J.M., Seguela, R., 2011. Crystallization behavior of carbon nanotube–polylactide nanocomposites. Macromolecules 44, 6496–6502.
Bocchini, S., Fukushima, K., Di Blasio, A., Fina, A., Frache, A., Geobaldo, F., 2010. Polylactic acid and polylactic acid-based nanocomposite photooxidation. Biomacromolecules 11, 2919–2926.
Cavallaro, G., Donato, D.I., Lazzara, G., Milioto, S., 2011a. Films of halloysite nanotubes sandwiched between two layers of biopolymer: from the morphology to the dielectric, thermal, transparency, and wettability properties. Journal of Physical Chemistry C 115, 20491–20498.
Cavallaro, G., Lazzara, G., Milioto, S., 2011b. Dispersions of nanoclays of different shapes into aqueous and solid biopolymeric matrices. Extended physicochemical study. Langmuir 27, 1158–1167.
Cho, K.H., Jang, B.S., Kim, K.H., Park, D.W., 2006. Performance of pyrophyllite and halloysite clays in the catalytic degradation of polystyrene. Reaction Kinetics and Catalysis Letters 88, 43–50.
Du, M., Guo, B., Jia, D., 2010. Newly emerging applications of halloysite nanotubes: a review. Polymer International 59, 574–582.
Fischer, E., Sterzel, H., Wegner, G., 1973. Investigation of the structure of solution grown crystals of lactide copolymers by means of chemical reactions Kolloid-Z. u. Z. Polymer 251, 980–990.
Hughes, A.D., King, M.R., 2010. Use of naturally occurring halloysite nanotubes for enhanced capture of flowing cells. Langmuir 26, 12155–12164.
Jiang, L., Zhang, J., Wolcott, M.P., 2007. Comparison of polylactide/nano-sized calcium carbonate and polylactide/montmorillonite composites: reinforcing effects and toughening mechanisms. Polymer 48, 7632–7644.
Joussein, E., Petit, S., Churchman, J., Theng, B., Righi, D., Delvaux, B., 2005. Halloysite clay minerals — a review. Clay Minerals 40, 383–426.
Kim, I.-H., Jeong, Y.G., 2010. Polylactide/exfoliated graphite nanocomposites with enhanced thermal stability, mechanical modulus, and electrical conductivity. Journal of Polymer Science Part B: Polymer Physics 48, 850–858.
Kontou, E., Niaounakis, M., Georgiopoulos, P., 2011. Comparative study of PLA nanocomposites reinforced with clay and silica nanofillers and their mixtures. Journal of Applied Polymer Science 122, 1519–1529.
Krikorian, V., Pochan, D.J., 2005. Crystallization behavior of poly(L-lactic acid) nanocomposites: nucleation and growth probed by infrared spectroscopy. Macromolecules 38, 6520–6527.
Lim, L.T., Auras, R., Rubino, M., 2008. Processing technologies for poly(lactic acid). Progress in Polymer Science 33, 820–852.
Liu, M., Guo, B., Du, M., Jia, D., 2007a. Drying induced aggregation of halloysite nanotubes in polyvinyl alcohol/halloysite nanotubes solution and its effect on properties of composite film. Applied Physics A: Materials Science & Processing 88, 391–395.
Liu, M.X., Guo, B.C., Du, M.L., Cai, X.J., Jia, D.M., 2007b. Properties of halloysite nanotube-epoxy resin hybrids and the interfacial reactions in the systems. Nanotechnology 18, 455703.
Lvov, Y.M., Shchukin, D.G., Mohwald, H., Price, R.R., 2008. Halloysite clay nanotubes for controlled release of protective agents. ACS Nano 2, 814–820.
Madhavan Nampoothiri, K., Nair, N.R., John, R.P., 2010. An overview of the recent developments in polylactide (PLA) research. Bioresource Technology 101, 8493–8501.
Matusik, J., Stodolak, E., Bahranowski, K., 2011. Synthesis of polylactide/clay composites using structurally different kaolinites and kaolinite nanotubes. Applied Clay Science 51, 102–109.
Murariu, M., Doumbia, A., Bonnaud, L., Dechief, A., Paint, Y., Ferreira, M., Campagne, C., Devaux, E., Dubois, P., 2011. High-performance polylactide/ZnO nanocomposites designed for films and fibers with special end-use properties. Biomacromolecules 12, 1762–1771.
Nel, A., Xia, T., Madler, L., Li, N., 2006. Toxic potential of materials at the nanolevel. Science 311, 622–627.
Purnama, P., Kim, S.H., 2009. Stereocomplex formation of high-molecular-weight polylactide using supercritical fluid. Macromolecules 43, 1137–1142.
Qi, R.L., Guo, R., Shen, M.W., Cao, X.Y., Zhang, L.Q., Xu, J.J., Yu, J.Y., Shi, X.Y., 2010. Electrospun poly(lactic-co-glycolicacid)/halloysite nanotube composite nanofibers for drug encapsulation and sustained release. Journal of Materials Chemistry 20, 10622–10629.
Qiao, J., Adams, J., Johannsmann, D., 2012. Addition of halloysite nanotubes prevents cracking in drying latex films. Langmuir 28, 8674–8680.
Ramontja, J., Ray, S.S., Pillai, S.K., Luyt, A.S., 2009. High-performance carbon nanotube-reinforced bioplastic. Macromolecular Materials and Engineering 294, 839–846.
Rasal, R.M., Janorkar, A.V., Hirt, D.E., 2010. Poly(lactic acid) modifications. Progress in Polymer Science 35, 338–356.
Ray, S.S., Bousmina, M., 2005. Biodegradable polymers and their layered silicate nanocomposites: In greening the 21st century materials world. Progress in Materials Science 50, 962–1079.
Ray, S.S., Okamoto, M., 2003. Biodegradable polylactide and its nanocomposites: opening a new dimension for plastics and composites. Macromolecular Rapid Communications 24, 815–840.
Rooj, S., Das, A., Thakur, V., Mahaling, R.N., Bhowmick, A.K., Heinrich, G., 2010. Preparation and properties of natural nanocomposites based on natural rubber and naturally occurring halloysite nanotubes. Materials and Design 31, 2151–2156.
Shchukin, D.G., Sukhorukov, G.B., Price, R.R., Lvov, Y.M., 2005. Halloysite nanotubes as biomimetic nanoreactors. Small 1, 510–513.
Shikinami, Y., Okuno, M., 1999. Bioresorbable devices made of forged composites of hydroxyapatite (HA) particles and poly-L-lactide (PLLA): part I. Basic characteristics. Biomaterials 20, 859–877.
Singh, S., Ray, S.S., 2007. Polylactide based nanostructured biomaterials and their applications. Journal of Nanoscience and Nanotechnology 7, 2596–2615.
Sperling, L., 2006. Introduction to Physical Polymer Science, 4th ed. John Wiley & Sons, Inc., Hoboken, New Jersey.
Sumi, K., Kobayashi, Y., Kato, E., 1998. Preparation of dense cordierite ceramics from ultrafine particles of magnesium hydroxide and kaolin. Journal of the Ceramic Society of Japan 106, 693–697.
Teng, C.-C., Ma, C.-C.M., Cheng, B.-D., Shih, Y.-F., Chen, J.-W., Hsiao, Y.-K., 2011. Mechanical and thermal properties of polylactide-grafted vapor-grown carbon nanofiber/polylactide nanocomposites. Composites Part A: Applied Science and Manufacturing 42, 928–934.
Turan, D., Sirin, H., Ozkoc, G., 2011. Effects of POSS particles on the mechanical, thermal, and morphological properties of PLA and plasticised PLA. Journal of Applied Polymer Science 121, 1067–1075.
Vergaro, V., Abdullayev, E., Lvov, Y.M., Zeitoun, A., Cingolani, R., Rinaldi, R., Leporatti, S., 2010. Cytocompatibility and uptake of halloysite cay nanotubes. Biomacromolecules 11, 820–826.
Verheyen, C., Wijn de, J., Blitterswijk van, C., Groot de, K., 1992. Evaluation of hydroxylapatite/poly(L-lactide) composites: mechanical behavior. Journal of Biomedical Materials Research 26, 1277–1296.
Wang, A.P., Kang, F.Y., Huang, Z.H., Guo, Z.C., Chuan, X.Y., 2008. Synthesis of mesoporous carbon nanosheets using tubular halloysite and furfuryl alcohol by a template-like method. Microporous and Mesoporous Materials 108, 318–324.
Wu, C.-S., Liao, H.-T., 2007. Study on the preparation and characterization of biodegradable polylactide/multi-walled carbon nanotubes nanocomposites. Polymer 48, 4449–4458.
Xu, J.-Z., Chen, T., Yang, C.-L., Li, Z.-M., Mao, Y.-M., Zeng, B.-Q., Hsiao, B.S., 2010. Isothermal crystallization of poly(L-lactide) induced by graphene nanosheets and carbon nanotubes: a comparative study. Macromolecules 43, 5000–5008.
Yuan, P., Southon, P.D., Liu, Z., Green, M.E.R., Hook, J.M., Antill, S.J., Kepert, C.J., 2008. Functionalization of halloysite clay nanotubes by grafting with gamma-aminopropyltriethoxysilane. Journal of Physical Chemistry C 112, 15742–15751.
Zhang, L., Liu, P., 2008. Facile fabrication of uniform polyaniline nanotubes with tubular aluminosilicates as templates. Nanoscale Research Letters 3, 299–302.
Zhou, S., Zheng, X., Yu, X., Wang, J., Weng, J., Li, X., Feng, B., Yin, M., 2007. Hydrogen bonding interaction of poly(D,L-lactide)/hydroxyapatite nanocomposites. Chemistry of Materials 19, 247–253.
Zhou, W.Y., Guo, B.C., Liu, M.X., Liao, R.J., Rabie, A.B.M., Jia, D.M., 2009. Poly(vinyl alcohol)/halloysite nanotubes bionanocomposite films: properties and in vitro osteoblasts and fibroblasts response. Journal of Biomedical Materials Research Part A 93A, 1574–1587.